JOURNAL OF COMPUTATIONAL PHYSICS 79, 70–84 (1988)

A Numerical Stability Analysis for the Two-Dimensional Incompressible Euler Equations

M. G. G. FOREMAN

Institute of Ocean Sciences, P.O. Box 6000, Sidney, British Columbia V8L 4B2, Canada

AND

A. F. BENNETT

College of Oceanography, Oregon State University, Corvallis, Oregon 97331

Received March 6, 1987; revised November 30, 1987

A normal mode analysis is used to determine the stability of a set of mixed hyperbolic/elliptic equations. The analysis is illustrated for a finite difference solution of the two-dimensional incompressible Euler equations on a rotating reference frame. The normal modes have a boundary layer structure which simplifies the analysis. One unstable and two stable sets of boundary conditions are analysed and the analysis results are confirmed with numerical experiments. © 1988 Academic Press, Inc.

INTRODUCTION

In the course of developing a two-dimensional nondivergent model of ocean circulation, a numerical instability was encountered. A series of experiments soon demonstrated that this instability arose from an unsuitable implementation of the boundary conditions. The original instability occurred with the full nonlinear equations, a spatially dependent Coriolis parameter, and rigid boundary conditions on all four sides of a rectangular domain. However an instability still occurs with linear equations, a constant Coriolis parameter, and boundaries which are periodic on the east and west and rigid on the north and south. Since this latter problem is much easier to analyse, it is the one considered in this study.

Most stability theory for finite difference models of hyperbolic initial boundary value problems is based on a classic yet complex paper by Gustafsson, Kreiss, and Sundström [1] (henceforth GKS). Unfortunately their normal mode analysis for stability is not applicable for this problem because one of our governing equations is elliptic. Although we make no attempt to extend GKS theory to our set of mixed hyperbolic/elliptic equations, we do demonstrate that with a combined normal mode and boundary layer analysis (that has some similarities to a GKS analysis),

0021-9991/88 $3.00

our unstable mode can be predicted with high accuracy! In particular, our analysis shows that the instability arises solely from the boundary conditions.

In addition to the one set of unstable boundary conditions, two other sets of boundary conditions are also analysed and shown to be stable. Numerical calculations and experiments confirm the analysis and indicate that these latter two conditions are also stable for the more complicated nonlinear problem. One of these stable conditions was chosen for our subsequent ocean circulation model experiments [2].

Though the analysis is illustrated for the nondivergent primitive equations as applied to ocean modelling, it should also be suitable for the incompressible Euler equations (e.g., Batchelor [3]) and their many applications. Furthermore, the analysis is not restricted to one particular finite difference scheme. An analysis similar to the one presented here suggests that boundary layers also govern the stability of our numerical model when the approximating finite difference scheme is based on an Arakawa B (e.g., Mesinger and Arakawa [4]) rather than an Arakawa C lattice.

Governing Equations

Governing equations for this problem are the two-dimensional linearized incompressible Euler equations on a rotating reference frame. In an oceanographic setting these equations are referred as the nondivergent primitive equations. Assuming linear drag and a constant Coriolis parameter, these equations are

$$\frac{\partial u}{\partial t} - fv + \frac{\partial p}{\partial x} + \tau u = F, \tag{1a}$$

$$\frac{\partial v}{\partial t} + fu + \frac{\partial p}{\partial y} + \tau v = G, \tag{1b}$$

$$\frac{\partial u}{\partial x} + \frac{\partial v}{\partial y} = 0, \tag{1c}$$

where

$u(x, y, t) = x$ component of velocity,

$v(x, y, t) = y$ component of velocity,

$p(x, y, t) =$ pressure per unit density,

$F(x, y) = x$ component of forcing,

$G(x, y) = y$ component of forcing,

$f =$ Coriolis parameter,

$\tau =$ bottom friction parameter.

These equations are solved on a rectangular domain with periodic boundary conditions at $x=0$ and $x=L_1$, and rigid (free-slip) boundary conditions (i.e., $v=0$) at $y=0$ and $y=L_2$.

In order to solve these equations numerically, (1c) may be replaced with a Poisson equation for p. This approach, rather than the more common stream-function-vorticity reformulation (e.g., Roache [5]), was chosen in order to avoid the calculation of a wall vorticity (see [2] for further details). In particular, taking $\partial(1a)/\partial x + \partial(1b)/\partial y$ and substituting (1c) yields

$$\frac{\partial^2 p}{\partial x^2}+\frac{\partial^2 p}{\partial y^2}-f\left(\frac{\partial v}{\partial x}-\frac{\partial u}{\partial y}\right)=\frac{\partial F}{\partial x}+\frac{\partial G}{\partial y}. \tag{2}$$

Neumann boundary conditions for (2) at $y=0$ and $y=L_2$ are obtained by substituting $v=0$ into (1b). They are

$$\frac{\partial p}{\partial y}+fu=G. \tag{3}$$

The Numerical Solution

Equations (1a), (1b), (2) are solved numerically with a finite difference method which uses an Arakawa C lattice [4] spatial discretization and leapfrog time-stepping. The spatial stencil is shown in Fig. 1.

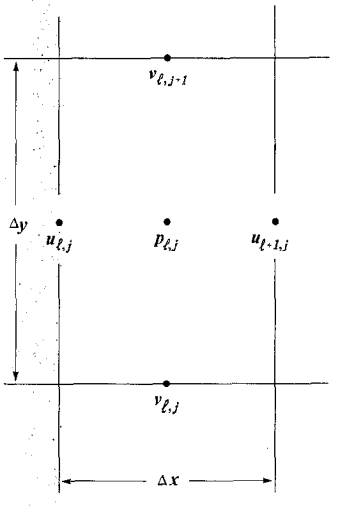

FIG. 1. Spatial stencil for the Arakawa C lattice.

Assuming $\Delta x = \Delta y$ and setting $l = 1$, M and $j = 1$, N as indices in the x, y directions, respectively, the finite difference equations corresponding to (1a), (1b) are

$$(u_{l,j}^{n+1} - u_{l,j}^{n-1})/2\Delta t - \tfrac{1}{4} f(v_{l,j}^n + v_{l,j+1}^n + v_{l-1,j}^n + v_{l-1,j+1}^n) + (p_{l,j}^n - p_{l-1,j}^n)/\Delta x + \tfrac{1}{2}\tau(u_{l,j}^{n+1} + u_{l,j}^{n-1}) = F_{l,j}^n, \tag{4a}$$

$$(v_{l,j}^{n+1} - v_{l,j}^{n-1})/2\Delta t + \tfrac{1}{4} f(u_{l,j}^n + u_{l+1,j}^n + u_{l,j-1}^n + u_{l+1,j-1}^n) + (p_{l,j}^n - p_{l,j-1}^n)/\Delta x + \tfrac{1}{2}\tau(v_{l,j}^{n+1} + v_{l,j}^{n-1}) = G_{l,j}^n. \tag{4b}$$

Rather than applying finite differences directly to (2), a specific equation is derived by combining (4a), (4b) with the following discretization of (1c)

$$(u_{l+1,j}^n - u_{l,j}^n + v_{l,j+1}^n - v_{l,j}^n)/\Delta x = 0. \tag{4c}$$

Taking the difference between (4c) at levels $n+2$ and n, and substituting from (4a), (4b) yields a finite difference approximation to (2),

$$\begin{aligned}(p_{l+1,j}^{n+1} + p_{l-1,j}^{n+1} + p_{l,j-1}^{n+1} + p_{l,j+1}^{n+1} - 4p_{l,j}^{n+1})/\Delta x^2 \\ - \tfrac{1}{4} f(v_{l+1,j+1}^{n+1} + v_{l+1,j}^{n+1} - v_{l-1,j+1}^{n+1} - v_{l-1,j}^{n+1})/\Delta x \\ + \tfrac{1}{4} f(u_{l+1,j+1}^{n+1} + u_{l,j+1}^{n+1} - u_{l+1,j-1}^{n+1} - u_{l,j-1}^{n+1})/\Delta x \\ = (F_{l+1,j}^{n+1} - F_{l,j}^{n+1} + G_{l,j+1}^{n+1} - G_{l,j}^{n+1})/\Delta x,\end{aligned} \tag{5}$$

that maintains discrete nondivergence. This Poisson equation is solved with the direct solver BLKTRI from the NCAR library [6].

The numerical implementation of boundary condition (3) is crucial for stability. We have followed two options. The first option, though more complicated in its derivation, produces the instability whose analysis forms the crux of this study. The second option is more straightforward and stable. However, we show that its stability can be predicted by the same analysis.

(I) The first and seemingly natural option is to impose a condition that is spatially centered over the outermost pressure point, rather than over the true boundary which lies half a grid interval beyond. Approximate Neumann conditions at these most northern and most southern p points are obtained by averaging Eq. (4b) for the v points on the boundary and one grid interval in from the boundary. For example, at the northern boundary where $j = N$ and $v_{l,N+1}^n = 0$ for all l and n, the Neumann condition derived in this manner is

$$\begin{aligned}\tfrac{1}{2}(p_{l,N+1}^{n+1} - p_{l,N-1}^{n+1})/\Delta x + \tfrac{1}{2}(v_{l,N}^{n+2} - v_{l,N}^n)/2\Delta t + \tfrac{1}{2}\tau(v_{l,N}^{n+2} + v_{l,N}^n) \\ + \tfrac{1}{2} f(u_{l,N+1}^{n+1} + u_{l+1,N+1}^{n+1} + 2u_{l,N}^{n+1} + 2u_{l+1,N}^{n+1} + u_{l,N-1}^{n+1} + u_{l-1,N-1}^{n+1})/4 \\ = \tfrac{1}{2}(G_{l,N+1}^{n+1} + G_{l,N}^{n+1}).\end{aligned} \tag{6}$$

The implementation of this condition has two snags. The first is that $p_{l,N+1}$, $u_{l,N+1}$, and $u_{l+1,N+1}$ are fictitious points beyond the northern boundary. This snag is overcome in the NCAR Poisson solver by combining (6) with (5). In particular, substituting for $p_{l,N+1}$ from (6) into (5), yields the following special version of (5) when $j=N$:

$$(p^{n+1}_{l+1,N}+p^{n+1}_{l-1,N}+2p^{n+1}_{l,N-1}-4p^{n+1}_{l,N})/\Delta x^2-\left(\frac{v^{n+2}_{l,N}-v^{n}_{l,N}}{2\Delta t}+\frac{1}{2}\tau(v^{n+2}_{l,N}+v^{n}_{l,N})\right)\Big/\Delta x$$
$$-f(u^{n+1}_{l,N}+u^{n+1}_{l+1,N}+u^{n+1}_{l,N-1}+u^{n+1}_{l+1,N-1})/2\Delta x-f(v^{n+1}_{l+1,N}-v^{n+1}_{l-1,N})/4\Delta x$$
$$=(F^{n+1}_{l+1,N}-F^{n+1}_{l,N}-2G^{n+1}_{l,N})/\Delta x. \tag{7}$$

Note that the $u_{l,N+1}$ and $u_{l+1,N+1}$ terms have cancelled. A similar special version of (5) is also used when $j=1$.

The second snag is that $v_{l,N}$ does not yet exist at time level $n+2$. Consequently it must be approximated. Two approximations were tried. The first was

$$\frac{(v^{n+2}_{l,N}-v^{n}_{l,N})}{2\Delta t}+\frac{1}{2}\tau(v^{n+2}_{l,N}+v^{n}_{l,N})\approx\frac{(v^{n+1}_{l,N}-v^{n-1}_{l,N})}{2\Delta t}+\frac{1}{2}\tau(v^{n+1}_{l,N}+v^{n-1}_{l,N}), \tag{8a}$$

and the second was

$$\frac{(v^{n+2}_{l,N}-v^{n}_{l,N})}{2\Delta t}+\frac{1}{2}\tau(v^{n+2}_{l,N}+v^{n}_{l,N})\approx\frac{(v^{n+1}_{l,N}-v^{n}_{l,N})}{\Delta t}+\frac{1}{2}\tau(v^{n+1}_{l,N}+v^{n}_{l,N}). \tag{8b}$$

When (8a) is substituted into (7) (and a similar approximation is used at $j=1$), the numerical model is stable. However, when approximation (8b) is used instead, the numerical model is unstable. Details of this instability and its associated analysis are given in the next section.

(II) The second option for implementing boundary condition (3) is to assume that the boundary for the discrete Poisson equation lies on the true boundary, $\Delta x/2$ beyond the outermost pressure point. The Neumann condition at the northern boundary, namely,

$$(p^{n+1}_{l,N+1}-p^{n+1}_{l,N})/\Delta x+\tfrac{1}{4}f(u^{n+1}_{l,N+1}+u^{n+1}_{l+1,N+1}+u^{n+1}_{l,N}+u^{n+1}_{l+1,N})=G^{n+1}_{l,N+1}, \tag{9}$$

is now obtained by setting $v_{l,N+1}=0$ in (4b). As before, the fictitious points $p_{l,N+1}$, $u_{l,N+1}$, and $u_{l+1,N+1}$ are eliminated by substituting from (9) into (5) when $j=N$. The special version of (5) now becomes

$$(p^{n+1}_{l+1,N}+p^{n+1}_{l-1,N}+p^{n+1}_{l,N-1}-3p^{n+1}_{l,N})/\Delta x^2$$
$$-f(u^{n+1}_{l,N}+u^{n+1}_{l+1,N}+u^{n+1}_{l+1,N-1}+u^{n-1}_{l,N-1})/4\Delta x-f(v^{n+1}_{l+1,N}-v^{n+1}_{l-1,N})/4\Delta x$$
$$=(F^{n+1}_{l+1,N}-F^{n+1}_{l,N}-G^{n+1}_{l,N})/\Delta x. \tag{10}$$

A similar equation can be derived when $j=1$. When condition (10) and its $j=1$ analog are used, the model is stable.

The major focus of this paper is the analysis of the numerical instability that arises when approximation (8b) is substituted into condition (7). However, the same analysis confirms the stability of boundary condition (10) and the condition that results when (8a) is combined with (7). These analyses are detailed in the next sections.

The Stability Analysis

The first step of our analysis is to assume solutions of the form

$$\begin{pmatrix} u_{l,j}^n \\ v_{l,j}^n \\ p_{l,j}^n \end{pmatrix} = \lambda^n \begin{pmatrix} U_j e^{i(l-1/2)\kappa} \\ V_j e^{il\kappa} \\ P_j e^{il\kappa} \end{pmatrix}, \tag{11}$$

where $j=1, N$; $l=1, M$; $i=(-1)^{1/2}$; κ is the wavenumber in the x direction; and U_j, V_j, P_j are complex-valued amplitudes. Since the eastern and western boundaries are periodic, κ can only assume a finite number of real values. In particular, if $\Delta x = L_1/(M-1)$ then

$$\kappa = \pm \frac{2\pi s}{M-1} \tag{12}$$

where $s=1, ..., (M-1)/2$.

The second step in our analysis is to assume a particular form for the amplitudes in (11). With reference to Fig. 2, normal velocities lying along the northern and southern boundaries are $v_{l,N+1}$ and $v_{l,1}$, respectively. They have the value zero. Amplitudes for the interior variables $v_{l,2}$, $u_{l,2}$, $p_{l,2}$, ..., $v_{l,N-1}$, $u_{l,N-1}$, $p_{l,N-1}$, $v_{l,N}$ are then assumed to have the form

$$\begin{pmatrix} U_j \\ V_j \\ P_j \end{pmatrix} = \sum_{\mu \in \mathscr{S}} \begin{pmatrix} U_0(\mu)\, e^{i(j-(N+1)/2)\mu} \\ V_0(\mu)\, e^{i(j-(N+2)/2)\mu} \\ P_0(\mu)\, e^{i(j-(N+1)/2)\mu} \end{pmatrix}, \tag{13}$$

where for a given κ, $\mathscr{S}$ is the set of all admissable complex wavenumbers μ in the y direction. No assumptions are made for the amplitudes P_N, U_N, P_1, U_1, associated with the boundary variables $p_{l,N}$, $u_{l,N}$, $p_{l,1}$, and $u_{l,1}$.

The third step of the analysis disregards the boundary conditions and finds admissable values for μ based on the assumed interior form of the solution. This step of the analysis is analogous to finding the Cauchy solution in a GKS analysis.

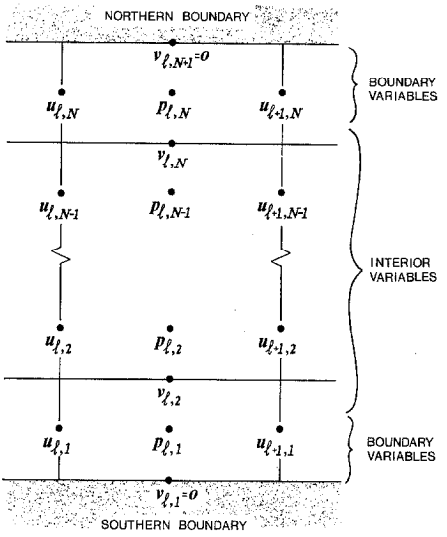

FIG. 2. Interior and boundary variables for the normal mode analysis.

Using these μ values and matching boundary and interior solutions, the amplitudes U_0, V_0, P_0, U_1, U_N, P_1, P_N, and the amplification factor, λ, can then be calculated.

Substituting (11) into (4a), (4b), and (5) yields the matrix equation

$$\mathbf{A}\begin{pmatrix} U_0 \\ V_0 \\ P_0 \end{pmatrix} = \mathbf{0}, \tag{14a}$$

where

$$\mathbf{A} = \begin{pmatrix} \dfrac{\lambda^2-1}{2\Delta t}+\dfrac{\tau}{2}(\lambda^2+1) & -f\cos(\kappa/2)\cos(\mu/2) & \dfrac{2i}{\Delta x}\sin(\kappa/2) \\ f\cos(\kappa/2)\cos(\mu/2) & \dfrac{\lambda^2-1}{2\Delta t}+\dfrac{\tau}{2}(\lambda^2+1) & \dfrac{2i}{\Delta x}\sin(\mu/2) \\ \dfrac{if}{\Delta x}\cos(\kappa/2)\sin\mu & -\dfrac{if}{\Delta x}\cos(\mu/2)\sin\kappa & \dfrac{2\cos\kappa+2\cos\mu-4}{\Delta x^2} \end{pmatrix}. \tag{14b}$$

For a nontrivial solution to (14) it is necessary that

$$\det(\mathbf{A}) = 0. \tag{15}$$

This is true when either

$$\lambda = \pm\{(1-\tau\,\Delta t)/(1+\tau\,\Delta t)\}^{1/2} \tag{16a}$$

or

$$\cos\kappa + \cos\mu - 2 = 0. \tag{16b}$$

Since κ is real, it follows that the interior solution which satisfies (16b) will have its y-directional wavenumber given by

$$\mu = i\cosh^{-1}(2 - \cos\kappa). \tag{17}$$

As the governing equations (1) do not have growing solutions when $\tau > 0$, numerical stability for the interior problem is ensured when

$$|\lambda| < 1. \tag{18}$$

(Note that condition (18) is stronger than GKS stability which requires $|\lambda| \leqslant 1 + O(\Delta t)$.) Furthermore since $\tau > 0$, (16a) implies that (18) is always satisfied. An unstable mode must therefore satisfy (17).

Notice, however, that (17) does not include λ and therefore (unlike what usually occurs for the Cauchy solution in a GKS analysis) does not lead to a stability constraint. This result is a direct consequence of the time independence of the Poisson equation. It means that an instability must arise from unsuitable boundary conditions.

The fourth step of our normal mode analysis finds the particular boundary and interior solutions that also satisfy the boundary conditions. From (17) note that for each κ, there are two admissable μ values, $\mu = \pm ib$ with $b > 0$. As given by (13), the separable form of the solution in the y direction is thus a linear combination of the terms $e^{(j-(N+1)/2)b}$ and $e^{-(j-(N+1)/2)b}$. Since the former term dominates at the northern boundary ($j = N$) and the latter term dominates at the southern boundary ($j = 1$), we need only consider one value of μ at each boundary. Hence, as is common in two-point boundary value analyses (e.g., Carrier and Pearson [7]), the effects of the boundaries can be isolated from each other.

Consider the northern boundary. Substituting (11) and (13) into the homogeneous version of (7) with approximation (8b) yields (to order $e^{-(N-1)b}$)

$$\begin{aligned}\lambda\left(\frac{2\cos\kappa - 4}{\Delta x^2}\right) P_N - \frac{f\lambda}{\Delta x}\cos(\kappa/2)\, U_N \\ = -\lambda\left(\frac{2e^{i(N-1)\mu}}{\Delta x^2}\right) P_0 + \frac{f\lambda}{\Delta x} U_0 e^{i(N-1)\mu}\cos(\kappa/2) \\ + \frac{e^{i(N-1/2)\mu}}{\Delta x} V_0\left(\frac{(\lambda-1)}{\Delta t} + \frac{1}{2}\tau(\lambda+1) + \frac{1}{2} f\lambda i \sin\kappa\right).\end{aligned} \tag{19}$$

Using $v_{I,N+1} = v_{I+1,N+1} = 0$, the same substitutions in (4a) and (4b) for $j = N$ yield (also to order $e^{-(N-1)b}$)

$$U_N\{(\lambda^2 - 1)/2\Delta t + \tfrac{1}{2}\tau(\lambda^2 + 1)\} + P_N(2i\lambda \sin(\kappa/2))/\Delta x = \tfrac{1}{2} f\lambda V_0 e^{i(N-1/2)\mu}\cos(\kappa/2), \tag{20}$$

and

$$\tfrac{1}{2}f\lambda U_N \cos(\kappa/2) + \lambda P_N/\Delta x = -V_0 e^{i(N-1/2)\mu}\{(\lambda^2-1)/2\Delta t + \tfrac{1}{2}\tau(\lambda^2+1)\} - \tfrac{1}{2}f\lambda U_0 e^{i(N-1)\mu}\cos(\kappa/2) + P_0\lambda e^{i(N-1)\mu}/\Delta x. \quad (21)$$

These three equations are combined with two from (14). For example, choosing the Poisson pressure equation (and using (16b)), and the u momentum equation we get

$$U_0 = \frac{\sin(\kappa/2)}{\sin(\mu/2)} V_0, \quad (22)$$

and

$$\{(\lambda^2-1)/2\Delta t + \tfrac{1}{2}\tau(\lambda^2+1)\}\, U_0 - f\lambda \cos(\kappa/2)\cos(\mu/2)\, V_0 + 2i\lambda \sin(\kappa/2)\, P_0 = 0. \quad (23)$$

There are now five equations in the six unknowns U_0, V_0, P_0, P_N, U_N, λ. After some algebra, U_0, P_0, P_N, and U_N can be expressed in terms of V_0 and λ provided

$$\lambda^4 + \alpha_3\lambda^3 + \alpha_2\lambda^2 + \alpha_1\lambda + \alpha_0 = 0, \quad (24)$$

for some complex coefficients α_3, α_2, α_1, α_0. The roots of this polynomial determine the amplification factors and the stability of the numerical solution. In particular, the root with the largest magnitude, $\lambda_{\max}$, will dominate the solution as n increases. If $|\lambda_{\max}| > 1$, the solution will be unstable.

A polynomial of the form (24) also arises when the southern boundary is considered in isolation. In fact, with the same κ and $\mu = ib$ rather than $\mu = -ib$, the amplification factors are the complex conjugates of those arising from the northern boundary. (With $-\kappa$ and $\mu = -ib$, the amplification factors for the southern boundary are the same as those for the northern boundary with κ and $\mu = ib$.) Consequently, both boundaries contribute equally to the instability.

The foregoing analysis may also be carried out for the two sets of stable boundary conditions. When (10) and its counterpart at the southern boundary are used, a fourth-order polynomial of the form (24) also arises. However, when (8a) is substituted into (7) and a similar condition is employed at the south, (24) becomes a fifth-order polynomial in λ.

Confirmation of the Analysis for the Unstable Boundary Conditions

The following test problems were chosen to demonstrate the accuracy of the preceding stability analysis. Periodic boundaries were placed on the east and west, and rigid boundaries were placed on the north and south of the rectangular domain. Common nondimensional parameters for both problems were $f = 1$,

$\tau = 0.01818$, $L_1 = 1$, $\Delta x = \Delta y = 1/(M-1)$, $F = G = 0$, while differing parameters were:

I. $M = 6$, $N = 7$, $\Delta t = 0.792$,

II. $M = 11$, $N = 15$, $\Delta t = 0.396$.

Uniform random numbers in the range $(-0.5, 0.5) \times 10^{-6}$ were specified for both u and v at time step 1, while zero values were assigned at time step zero. The associated pressure field at time step 1 was calculated using (5). Constant extrapolation of velocity u (i.e., a no-shear condition) was assumed for evaluating the Coriolis terms in equation (4b) adjacent to the rigid boundaries.

These two test models were run for $400\Delta t$ and $800\Delta t$, respectively; u, v, p values over the last $50\Delta t$ were stored at all grid points. In both cases, the model was clearly seen to be going unstable at a uniform growth rate. A least squares analysis of all time series over the last $50\Delta t$ was then performed to determine the form of the unstable mode. This analysis proceeds as follows.

Based on the normal mode analysis at the northern and southern boundaries, solutions of the form

$$\begin{pmatrix} u_{l,j}^n \\ v_{l,j}^n \\ p_{l,j}^n \end{pmatrix} = \begin{pmatrix} u_j \\ v_j \\ p_j \end{pmatrix} \lambda^n e^{il\kappa} + \begin{pmatrix} u_j^* \\ v_j^* \\ p_j^* \end{pmatrix} (\lambda^*)^n e^{-il\kappa} + \begin{pmatrix} \bar{u}_j \\ \bar{v}_j \\ \bar{p}_j \end{pmatrix} \lambda^n e^{-il\kappa} + \begin{pmatrix} \bar{u}_j^* \\ \bar{v}_j^* \\ \bar{p}_j^* \end{pmatrix} (\lambda^*)^n e^{il\kappa} \tag{25}$$

were assumed; * denotes complex conjugate,

$$\lambda = re^{i\theta} \tag{26}$$

is the amplification factor, and u_j, v_j, p_j, $\bar{u}_j$, $\bar{v}_j$, $\bar{p}_j$ are complex amplitudes. The value of λ at each grid point was then found by fitting the nonlinear function

$$u_{l,j}^n = r^n [B_{l,j} \cos(n\theta) + C_{l,j} \sin(n\theta)] \tag{27}$$

to each u time series, and similar functions to the v and p time series. Parameters in the fit are r, θ, $B_{l,j}$, and $C_{l,j}$. Although the values of $B_{l,j}$ and $C_{l,j}$ changed for each (l, j), for all variables the values

$$\lambda = 1.09973 e^{i2.85631} \tag{28a}$$

and

$$\lambda = 1.04217 e^{i2.98576} \tag{28b}$$

emerged for test problems I and II, respectively. And in all cases the residuals after the fit were very small.

Subsequent analyses of the $B_{l,j}$, $C_{l,j}$ fields were then performed to determine the spatial form of the unstable mode. Substituting

$$u_j = Q_j + iR_j = S_j e^{i\phi_j} \tag{29a}$$

$$\bar{u}_j = \bar{Q}_j + i\bar{R}_j = \bar{S}_j e^{i\bar{\phi}_j} \tag{29b}$$

into (25) reveals that

$$B_{l,j} = (Q_j + \bar{Q}_j)\cos(l\kappa) + (-R_j + \bar{R}_j)\sin(l\kappa), \tag{30a}$$

$$C_{l,j} = (-Q_j + \bar{Q}_j)\sin(l\kappa) - (R_j + \bar{R}_j)\cos(l\kappa). \tag{30b}$$

So the next stage of the analysis required fitting along each row j of the $B_{l,j}$ and $C_{l,j}$ arrays, functions of the form (30). In this case, the unknown parameters are S_j, $\bar{S}_j$, ϕ_j, $\bar{\phi}_j$, and κ. For all variables and along all rows, the values

$$\kappa = 2\pi/5 \tag{31a}$$

and

$$\kappa = 6\pi/10 \tag{31b}$$

were found for problems I and II, respectively. The residuals from each fit were again very small.

The unstable mode for each of the u, v, p variables therefore has a single amplification factor λ and a single wavenumber κ in the x direction. Furthermore, the values are predicted "exactly" by the normal mode analysis. In particular, when all the roots of (24) are calculated for all possible real κ values, the largest $\lambda_{\max}$ has the value given by (28) and is associated with the κ given by (31). The values agree to at least 4 digits.

The y-directional form of the unstable mode is given by the S_j, $\bar{S}_j$, ϕ_j, $\bar{\phi}_j$ values that emerge from fits to $B_{l,j}$ and $C_{l,j}$. Table I shows these values for u for problem I.

TABLE I

Parameters for the Unstable Mode in the y Direction

j	S_j	ϕ_j	$\bar{S}_j$	$\bar{\phi}_j$
1	0.71544×10^{-6}	−2.8593	0.45328×10^{-2}	0.7646
2	0.16307×10^{-5}	−3.0496	0.43700×10^{-3}	2.8400
3	0.39765×10^{-5}	−3.0769	0.14311×10^{-3}	2.8401
4	0.11818×10^{-4}	−3.0807	0.46991×10^{-4}	2.8405
5	0.35993×10^{-4}	−3.0811	0.15811×10^{-4}	2.8443
6	0.10991×10^{-3}	−3.0812	0.64838×10^{-5}	2.8716
7	0.11400×10^{-2}	1.1266	0.28447×10^{-5}	3.0620

When (31a) is substituted in (17) we get

$$\mu = \pm i 1.11665. \tag{32}$$

Consequently if the interior solution is described by (11) and (13), we should have

$$\frac{S_j}{S_{j+1}} = e^{-1.11665} = 0.327375, \tag{33a}$$

and

$$\frac{\bar{S}_j}{\bar{S}_{j+1}} = e^{1.11665} = 3.05460. \tag{33b}$$

Table I shows that both relationships are approximately true. Discrepancies are larger for the smaller S_j and $\bar{S}_j$ values but this is probably attributable to the limits of machine precision, errors arising from the two least squares fits, and the assumption that the two boundaries can be considered in isolation.

The normal mode analysis also predicts correctly the numerical solution in the boundary layer. In particular,

$$\frac{u_7}{u_6} = \frac{U_7}{U_0 e^{2 * 1.11665}} \tag{34a}$$

and

$$\frac{\bar{u}_1}{\bar{u}_2} = \frac{U_1}{U_0 e^{-2 * 1.11665}}. \tag{34b}$$

to 4 digits. There is similar agreement between the normal mode and numerical results for problem II.

Confirmation of the Analysis for the Stable Boundary Conditions

When problems I and II are run with the two stable boundary conditions, namely,

(i) (10) and its $j = 1$ analog,

(ii) (7) with approximation (8a) and its $j = 1$ analog,

it is much more difficult to recover $\lambda_{\max}$. This is because there are several λ values that are very close in magnitude. Therefore a different approach is required to verify the amplification factors predicted by the normal mode analysis. The following tactic is adopted.

Assume that (4a), (4b), (5) have solutions of the form given by (11). Substituting

(11) into the homogeneous difference equations away from the northern and southern boundaries yields

$$\{\lambda(1+\tau\,\Delta t)-\lambda^{-1}(1-\tau\,\Delta t)\}u_j/2\Delta t - \tfrac{1}{2}f\cos(\kappa/2)(v_j+v_{j+1})+2i\sin(\kappa/2)\,p_j/\Delta x=0, \tag{35a}$$

$$\{\lambda(1+\tau\,\Delta t)-\lambda^{-1}(1-\tau\,\Delta t)\}v_j/2\Delta t + \tfrac{1}{2}f\cos(\kappa/2)(u_j+u_{j-1})+(p_j-p_{j-1})/\Delta x=0, \tag{35b}$$

$$\{2(\cos\kappa-2)\,p_j+p_{j+1}+p_{j-1}\}/\Delta x^2-\tfrac{1}{2}fi\sin\kappa(v_j+v_{j+1})/\Delta x + \tfrac{1}{2}f\cos(\kappa/2)(u_{j+1}-u_{j-1})/\Delta x=0. \tag{35c}$$

Similar substitutions are also made for the special versions of these equations adjacent to the northern and southern boundaries.

Defining

$$\mathbf{z}^t=(u_1,\,p_1,\,v_2,\,u_2,\,p_2,\,\ldots,\,u_N,\,p_N), \tag{36}$$

Eq. (35) and its counterparts at the boundary can be written in matrix form as

$$B\mathbf{z}=\mathbf{0}. \tag{37}$$

For a nontrivial solution, it is necessary that

$$\det(B)=0. \tag{38}$$

(Note the normal mode analysis also solves (37) by assuming amplitudes of the form (13) for the interior variables. This matrix approach is more general.) Since the numerical value of a matrix determinant varies with the matrix scaling, we replace (38) with the equivalent condition,

$$\gamma=0 \tag{39}$$

for at least one eigenvalue γ of B. So the amplification factors λ are precisely those values that cause at least one eigenvalue of B to satisfy (39). Calculation of these λs proceeds as follows.

Assume specific values of f, τ, Δx, Δt, N, and M. For all possible real values of κ and initial values of λ that are close but not identical to those predicted by the normal mode analysis, solve the problem

$$\text{minimize } |\gamma_{\min}| \text{ with respect to } \lambda,$$

where $\gamma_{\min}=$ the eigenvalue of $B(\lambda)$ with the smallest magnitude.

The solution to this problem is found using NAG [8] eigenvalue and unconstrained optimization routines. In all cases, the minimization confirmed that the amplification factors predicted by the normal mode analysis do cause B to have

a zero eigenvalue. In particular, with boundary condition (10) and both problems I and II, the normal mode analysis predicts that all the amplification factors are given by (24) and its analog at the southern boundary. This is confirmed by the eigenvalue solution to (38). When approximation (8a) is substituted into boundary condition (7) and a similar condition is used at the southern boundary, the normal mode analysis predicts the following amplification factors for problem I:

(i) when $\kappa = 2\pi/5$; $\lambda = \pm 0.985702$, $0.985922e^{-i0.001768}$, $0.992472e^{i2.99197}$, $0.244897e^{i0.151394}$,

(ii) when $\kappa = 4\pi/5$; $\lambda = \pm 0.985702$, $0.985729e^{-i0.000622}$, $0.987139e^{i3.07866}$, $0.155194e^{i0.063555}$.

Again all these values are confirmed by the eigenvalue solution to (38).

The amplification factors (both stable and unstable) that arise when using approximation (8b) in boundary condition (7) (and its counterpart at the southern boundary) were also confirmed with the eigenvalue solution to (38).

Summary and Conclusions

It has been demonstrated that with a combined normal mode and boundary layer analysis (that has some similarities to a GKS analysis), the numerical stability of a set of mixed hyperbolic/elliptic equations can be determined. In particular, it is shown that the numerical solution of the sample ocean circulation problem is characterized by the existence of a numerical boundary layer, and the revised stability analysis requires special treatment there. The general interior solution is shown to be unconditionally stable in the absence of boundaries. Instability is thus governed by the choice of boundary conditions. One set of unstable and two sets of stable boundary conditions are analysed. The amplification factors predicted by the normal mode analysis are confirmed by either running a numerical model and finding the unstable mode, or numerically calculating the eigenvalues of a matrix associated with the entire grid.

Though the analysis is illustrated for the nondivergent primitive equations as applied to ocean modelling, it should also be suitable for the Euler equations and their many applications. Furthermore, the analysis need not be restricted to finite difference schemes based on an Arakawa C lattice. An analysis similar to the preceding one suggests that boundary layers also exist and govern the numerical stability when Eqs. (1a), (1b), and (2) are approximated with a finite difference scheme that uses an Arakawa B lattice.

Acknowledgments

We thank Professor J. M. Varah for helpful comments and discussion and the reviewers for their constructive criticism of an earlier version of this paper.

REFERENCES

1. B. GUSTAFSSON, H. O. KREISS, AND A. SUNDSTRÖM, *Math. Comput.* **26**, 649 (1972).
2. M. G. G. FOREMAN AND A. F. BENNETT, *Dyn. Atmos. Oceans*, in press.
3. G. BATCHELOR, *An Introduction to Fluid Dynamics* (Cambridge Univ. Press, London, 1970).
4. F. MESINGER AND A. ARAKAWA, Numerical Methods Used in Atmospheric Models, Vol. 1, WMO-ICSU Joint Organizing Committee, GARP Publication Series Vol. 17, 1976 (unpublished).
5. P. J. ROACHE, *Computational Fluid Dynamics* (Hermosa, Albuquerque, NM, 1976).
6. P. SWARZTRAUBER AND R. SWEET, Efficient FORTRAN Subprograms for the Solution of Elliptic Partial Differential Equations, NCAR Technical Note NCAR-TN/IA-109, Boulder, 1975 (unpublished).
7. G. F. CARRIER AND C. E. PEARSON, *Partial Differential Equations, Theory and Technique* (Academic Press, New York, 1976).
8. Numerical Algorithms Group Library, NAG (USA) Inc., Downers Grove, IL.